The infectivity of SARS-CoV-2 progeny virions requires the activity of host cell N-myristoyltransferases and it is severely compromised by their inhibition

Saber H. Saber[1,2], Ravi Ojha[3], Tania Quirin[3], Janika Ruuska[3], Tomas Strandin[3,4], Ravi Kant[4,5], Lauri Kareinen[4,5], Nyakuoy Yak[1,2], Tarja Sironen[4,5], Olli Vapalahti[4,5,6], Giuseppe Balistreri[2,3]*, and Merja Joensuu[1,2]*

[1] Australian Institute for Bioengineering and Nanotechnology, The University of Queensland, Brisbane, Australia

[2] Queensland Brain Institute, The University of Queensland, Brisbane, Australia

[3] Faculty of Medicine, Medicum Research Program, University of Helsinki, Helsinki, Finland

[4] Department of Veterinary Biosciences, University of Helsinki, Helsinki, Finland

[5] Department of Virology, University of Helsinki, Helsinki, Finland

[6] HUS Diagnostic Center, Clinical Microbiology, Helsinki University Hospital, University of Helsinki, Helsinki, Finland

*Corresponding authors: m.joensuu@uq.edu.au , giuseppe.balistreri@helsinki.fi

Abstract

Acute respiratory syndrome coronavirus 2 (SARS-CoV-2) is the causative agent of the COVID-19 pandemic. Despite vaccinations, the development and use of neutralizing antibodies against the viral surface spike proteins, and small molecule inhibitors targeting the viral replication machinery, COVID-19 remains a global public health crisis. Emerging mutations in the viral genome have the potential to reduce prophylactic and therapeutic efficacy of virus-directed treatments. Targeting host cell factors required for infection could, therefore, be a potential strategy to overcome this problem since mutations in the viral genome are unlikely to bypass the requirement for the targeted host factor or function. The enzymatic activity of N-myristoyltransferases (NMTs) are essential to mediate stable membrane binding and function of a diverse class of cellular proteins, many of which regulate intracellular membrane trafficking. Here we report that nanomolar concentrations of the NMT inhibitor IMP-1088 inhibited SARS-CoV-2 spreading in human cells by compromising the infectivity of released viral particles, which was reduced by up to 90%. IMP-1088 also inhibited human Respiratory syncytial virus, the main cause of viral death in infants world-wide, but not the mosquito-delivered alphavirus Semliki Forest virus and the vesiculovirus Vesicular stomatitis virus. The antiviral effect of IMP-1088 against SARS-CoV-2 displayed remarkably slow reversibility, was well tolerated by cells, and is, therefore, a promising candidate for COVID-19 prophylaxis and therapy.

Introduction

The infection cycle of SARS-CoV-2, the causative agent of the COVID-19 pandemic, starts with the binding of the viral surface trimeric protein spike (S) to the main cell surface receptor angiotensin-converting enzyme 2 (ACE2) [1]. Once attached to the cell, the S must be cleaved by cellular proteases to undergo a conformational change that leads to the fusion of the viral lipid envelope with the membrane of the cell [2]. This fusion event results in the delivery of the viral genome in the cytoplasm of the cell. The cleavage of the viral S is performed by serine proteases such as TMPRSS2, localized at the cell surface or early endosomes [3], or by cysteine proteases such as Cathepsin-L, localized in the lumen of lysosomes [4]. Upon delivery into the cytoplasm of the target cell, the mRNA-like viral genome is translated by the ribosomes to produce the viral replication machinery [5]. This multiprotein complex, in turn, recruits the newly translated RNA genome to the endoplasmic reticulum membranes where virus-induced membrane enclosed compartments are then formed [5,6]. Inside these compartments the viral genome is first copied into a complementary strand, which serves as a template for shorter mRNA-like transcripts, the sub-genomic RNAs, as well as for the synthesis of full-length viral genomes that are released into the cytoplasm [5,6]. Among the genes encoded by the sub-genomic mRNAs are the four viral structural proteins, Spike (S), Envelope (E) and Membrane (M) protein, which are inserted in the viral envelope membrane, and the nucleoproteins (N) that bind to the newly synthesized viral RNA genomes to form a ribonucleoprotein complex [5]. The assembly of new progeny virions occurs at the cytosolic side of membranes of the endoplasmic reticulum Golgi intermediate compartment (ERGIC) [7]. The virions that initially bud into the lumen of the ERGIC are then released into the extracellular space by a process that is not completely understood and might involve transport through the Golgi and/or lysosomes, before secretion.

N-myristoylation is a lipidic co- or post-translational modification of proteins that is catalysed by the enzyme *N*-myristoyltransferases (NMT-1 and -2). Protein myristoylation is one of the ways that cells use to anchor proteins into membranes where they carry their function [8]. The most common type of myristoylation occurs at N-terminal glycine of the protein, at a consensus motive (M)GXXXXS_6 (M is methionine, G glycine, X any amino acid, and S serine). However, myristoylation can also occur at an internal amino acid residue when a protein is proteolytically cleaved exposing a G or K at the new N-terminus of one of the cleavage products [8,9]. In humans, NMTs exists in two isoforms, NMT-1 and -2, which are highly conserved across all mammalians [10,11].

The life cycle of several pathogens, including various bacteria and viruses, has been shown to depend on protein N-myristoylation [12]. While parasites like Plasmodium and Trypanosoma encode their own NMTs, some viruses depend on the activity of host NMTs. N-myristoylation of viral proteins is observed or predicted in families ranging from RNA to large DNA viruses, including *Picornovirdae, Arenaviridae, Reoviridae, Hepadnaviridae, Polyomaviridae, Ascoviridae, Herpesviridae, Poxviridae, Asfiviridae,* and *Iridoviridae* [12]. In all reported cases, the antiviral effect of NMT inhibitors has been attributed to the prevention of direct myristoylation of viral proteins [13-15].

The genome of SARS-CoV-2 does not harbour sequences encoding for obvious myristoylation sites and whether the proteins of SARS-CoV-2 are myristoylated is currently not known. However, we hypothesized that inhibiting cellular NMTs could interfere with one or more steps of the virus life cycle. To this end, we tested the antiviral potential of IMP-1088, a potent inhibitor of cellular NMT-1 and -2 [13]. The results demonstrate a strong SARS-CoV-2-specific antiviral activity of the drug, which is caused by the loss of infectivity of the virions released from IMP-1088-treated cells.

Results

Inhibition of cellular NMT-1 and -2 inhibits SARS-CoV-2 infection in human cells.

To test whether the inhibition of cellular NMT-1 and -2 affected any steps of SARS-CoV-2 life cycle, a broad range of IMP-1088 concentrations was used against a clinical isolate of SARS-CoV-2 corresponding to the ancestral Wuhan (Wuh) strain in human A549 lung small carcinoma cells that were engineered to stably express the virus receptor ACE2 and the protease TMPRSS2, the proteolytic activity of which is required to prime the viral S protein for fusion (here named A549-AT cells).

A549-AT cells were infected with SARS-CoV-2 Wuh using a multiplicity of infection (MOI) sufficient to infect approximately 20% of cells at 20 h post infection (hpi), which was equivalent to MOI=0.2 i.u./cell in VeroE6-TMPRSS2 cells (see methods). In these initial experiments, 20 h was chosen as the end point as it was a sufficient time to allow 2 to 3 rounds of infection. Cells were treated with increasing concentrations of IMP-1088 or DMSO control (vehicle) at 1.5 h before infection (hbi) or 1.5 h post infection (hpi) (Figure 1A). Following fixation, cells were processed for indirect immunofluorescence staining using antibodies raised against the N protein, and long (>40 base pairs) double stranded RNA (dsRNA) molecules, which are the hallmark of viral RNA replication (Figure 1 B). Using high-content imaging followed by automated image analysis, we quantified the number of N and dsRNA positive cells (as a readout of infectivity), as well as the fluorescence intensity of N and dsRNA labelling in each infected cell (as a readout of viral protein synthesis and viral RNA replication). Quantitative image analysis revealed that treatments with nanomolar concentrations of IMP-

1088 reduced infection to approximately 50% of the values obtained from vehicle control (DMSO) (Figure 1 B-D). A similar inhibitory profile was observed whether the drug was provided at 1.5 hbi or at 1.5 hpi (Figure 1 B-D), the latter being a time sufficiently long to allow virus entry and delivery of viral genomes into the cytoplasm of the target cell [3]. Notably, at a later time point (48 hpi), the antiviral effect of IMP-1088 was even stronger, reaching an inhibitory effect of up to 80-90% compared to DMSO vehicle control (Figure 1 E and F). The fluorescence intensity of N and dsRNA staining in each infected cell was similar following IMP-1088- and DMSO-treatment (Supplementary Figures 1 A and B), indicating that all the steps of the virus life cycle from entry to genome replication were not strongly inhibited by the drug treatment. IMP-1088 inhibited not only virus spreading in the cell culture within the 48 h observation time, but it also prevented virus-induced cell-to-cell fusion (known as syncytia) (Figure 1 E: the enlarged inset i shows a multi-nucleated syncytium of cells, and ii/ iii show infected single cells). The cytotoxic effect of IMP-1088 was assessed in A549-AT cells after 24 h of IMP-1088 treatment and no significant adverse effects were observed on the cell viability compared to the vehicle control (Figure 1 G). Taken together, these results suggest that the inhibition of cellular NMT1 and -2 interferes with one or more 'late' steps of the SARS-CoV-2 life cycle.

Inhibition of cellular NMT-1 and -2 does not interfere with early steps of the SARS-CoV-2 infection cycle.

The experiments presented above suggest that the 'early' steps of the virus life cycle are not strongly affected by the pre-treatment of cells with the NMT-1 and -2 inhibitor IMP-1088. To confirm this, we repeated the experiments fixing cells at the earlier time point of 8 hpi, which is sufficient to allow one round of infection (Figure 2 A). Supporting our earlier results (Supplementary Figures 1 A and B), pre-treatment of A549-AT cells with 0.1 µM or 1 µM IMP-1088 did not inhibit virus entry, viral protein synthesis or RNA replication (Figure 2 B-E; Supplementary Figures 1 C and D). Unlike IMP-1088, a pre-treatment with an inhibitor of endocytosis, 4OH-dynasore, previously shown to prevent SARS-CoV-2 cell entry [16], inhibited virus infection significantly at this time point (Figures 2 F and G). Thus, the antiviral effect of IMP-1088 is due to an interreference in a step of SARS-CoV-2 infection that follows genome replication.

IMP-1088 inhibits infection of SARS-CoV-2 variants Delta and Omicron, and Respiratory syncytial virus but not Semliki Forest or Vesicular stomatitis virus.

To test if inhibiting cellular NMT-1 and -2 resulted in an equally effective antiviral effect on SARS-CoV-2 Delta and Omicron variants of concern, A549-AT cells were infected as described above and, following a treatment with 0.1 µM and 1 µM IMP-1088 or DMSO control

for 24 h and 48 h, the samples were prepared for immunofluorescence analysis (Figure 3 A). Inhibition of NMT-1 and -2 reduced the number of Omicron and Delta N-positive cells (Figure 3 B-G) similarly to the Wuh ancestral strain (Figure 1 B-F).

To date, the antiviral activity of IMP-1088 has been demonstrated against the common cold rhinovirus, vaccinia virus, and yellow fever virus [13-15]. All these viruses harbour one or more proteins that undergo N-myristoylation. However, because inhibition of NMTs affects a large number of cellular proteins that could potentially regulate one or more steps of a virus life cycle, we tested the antiviral potential of IMP-1088 against three different membrane-enveloped viruses that do not, based on current knowledge, express myristoylated proteins: Semliki Forest virus (SFV, family *Togaviridae*), Vesicular stomatitis virus (VS, family *Rhabdoviridae*), and Respiratory syncytial virus (RSV, family *Pneumoviridae*). The three viruses have been previously engineered to express green fluorescent protein (GFP) as a reporter gene: SFV-GFP, VSV-GFP, RSV-GFP [17-19]. We first tested whether IMP-1088 interfered with the early steps of the virus life cycle. A549 cells, which are susceptible to the three viruses, were pre-treated with different concentrations of IMP-1088 added to cells 2 hbi or 1 hpi (Figure 4 A). Cells were infected with an amount of virus sufficient to infect 15-30% cells at 7 hpi (SFV-GFP and VSV-GFP), or 16 hpi (RSV-GFP). At these time points, GFP-positive fluorescence signal is detectable only in cells that have undergone the first round of infection. Image analysis revealed that IMP-1088 treatment had no effect on the infection of each of the three viruses at this early time points (Supplementary Figure 2). However, when cells were infected with lower doses of viruses and the infection period was extended for longer times to allow multiple rounds of infection, treatments with 0.01-1 μM IMP-1088 inhibited the infection of RSV-GFP by more than 50% compared to DMSO control at 48 hpi (Figure 4 B-E). SFV-GFP and VSV-GFP, on the other hand, were not affected by the drug treatment at 12 hpi, a time sufficiently long for these viruses to undergo multiple rounds of infection (Figure 4 F-M). In summary, inhibition of cellular NMTs by the small molecule IMP-1088 does not interfere with the early steps of the life cycle of all four viruses tested, but it does selectively inhibit SARS-CoV-2 and RSV-GFP at later times of infection.

The reversibility of the IMP-1088 antiviral activity is slow.

Towards the potential use of NMT-1 and -2 inhibitor as an antiviral agent, we tested the reversibility of the IMP-1088 antiviral activity in cell cultures. To this end, A549-AT cells were pre-treated with different concentrations of the drug, or DMSO control, for two hours and infected with SARS-CoV-2 Wuh. After 2h of infection, cells were washed and maintained in growth media with or without the drug. At 24 and 48 hpi, cells were fixed and processed for immunofluorescence staining against N as described above (Figure 5 A). Consistent with the extremely low dissociation constant reported for this drug (Kd< 210 pM) [13], our results indicate

that at 24 hpi (Figure 5B-C) and 48 hpi (Figure 5D-F), the antiviral effect of IMP-1088 is virtually irreversible at 1 μM.

Inhibition of cellular NMT-1 and -2 does not interfere with SARS-CoV-2 virion release.

The IMP-1088 inhibition of SARS-CoV-2 infection observed at 24 hpi and 48 hpi could be due to perturbation of one or more late steps of the virus life cycle, including assembly of new progeny virus, release of virions, and infectivity of the viral particles released from the drug-treated cells. To test these possibilities, we first determined by quantitative real time PCR (qRT-PCR) the extent of viral RNA release over time from A549-AT cells pre-treated with IMP-1088 or DMSO control. For the qRT-PCR we used primers directed against a portion of the viral RNA encoding for the RNA-dependent RNA polymerase (RdRp). For this, DMSO control and IMP-1088-treated A549-AT cells were infected with SARS-CoV-2 Wuh for 2 h and the culture media was then collected and analysed by qRT-PCR at 0 (i.e., directly after infection), 6, 12, 24, and 48 hpi (Figure 6 A). No difference in the viral RNA copy number in the collected media was detected up to 12 h post infection (Figures 6 B and D). Starting at 24 hpi and even more so at 48 hpi, the amounts of viral RNA that accumulated in the extracellular media of IMP-1088-treated cells progressively decreased, reaching levels approximately 10 times lower at 48 hpi compared to those obtained from cells treated with DMSO vehicle control (Figures 6 C and E). This late time point corresponds to multiple rounds of cell-to-cell infection. Because no differences were observed at earlier time points, the lower levels of extracellular viral RNA that were observed to accumulate at 48 hpi in IMP-1088 treated cells could be due to an impairment of virion infectivity, resulting in slower kinetics of cell-to-cell infection. This possibility was investigated next.

SARS-CoV-2 virions released from IMP-1088-treated cells are less infectious.

As schematized in Figure 7 A, to determine if virions released from IMP-1088-treated cells were less infectious compared to those released from cells treated with DMSO control, the extracellular media from SARS-CoV-2 Wuh infected A549-AT cells were collected at 48 hpi and used to re-infect highly susceptible VeroE6 cells. In short, the virus-producing A549-AT cells were first pre-treated starting 2 hbi with either DMSO control or with indicated concentrations of IMP-1088, which was then either washed out at 2 hpi (Figure 7 A, Wash out), or kept in the culture media for the duration of the experiment (Figure 7 A, No wash). Virus-containing media were collected at 48 hpi and the amount of viral RNA in each sample was quantified by qRT-PCR. VeroE6 cells were then infected in 96-well imaging plates with viral inocula containing equal amounts of viral RNA (Figure 7 A, qRT-PCR and VeroE6 cell reinfection). At 20 hpi, VeroE6 cells were fixed, and the number of infected cells was determined after immunofluorescence imaging and image analysis (Figure 7 A). The

quantification revealed that while VeroE6 cells were inoculated with media containing an equal amount of SARS-CoV-2 RNA genome copies, the virions that were released from IMP-1088-treated A549-AT cells were significantly less infectious compared to DMSO control (Figure 7 B-E). The decreased infectivity of the virions was observed across the different IMP-1088 treatments, both when the drug was washed off (Figures 7 B and C) or if it was left in the culture media, resulting in up to 90% inhibition of infection (Figures 7 D and E). Taken together, the results presented here indicate that inhibiting cellular NMTs with the small molecule IMP-1088 has no significant effect on the early steps of SARS-CoV-2 infection or virion release, but rather impairs the infectivity of newly released progeny virions.

Discussions

In general, vaccines can prevent serious disease and death, but they cannot prevent infection or contagion. The consequent rise of immune-resistant variants, the challenge of delivering vaccines in developing countries, and the fraction of the global population that does not want to or cannot be vaccinated urges the development of alternative prophylactic and curative strategies.

Current antiviral therapies against SARS-CoV-2 are based on systemically delivered (i.e., oral or intravenous administration) molecules that directly target viral components, such as neutralizing monoclonal antibodies, small molecule compounds that interfere with viral RNA synthesis (e.g., remdesivir, molnupiravir), or inhibitors of viral proteases (e.g., paxlovid). The use and efficacy of all these treatments is limited by several factors: the rise of drug-resistant virus mutants, the effective drug concentration at the site of infection (i.e., the respiratory tract) that can be achieved by systemic administration, the bioavailability of each compound, and by the potential side effects. Targeting the host rather than the virus, i.e., inhibiting multiple cellular factors or functions that are required for virus infection, would in principle limit the rise of drug-resistant virus mutants.

With this rationale in mind, we tested IMP-1088, an inhibitor of cellular NMT-1 and 2, against SARS-CoV-2, RSV, SFV, and VSV infections. We found that in cells treated with IMP-1088, the late steps of both SARS-CoV-2 and RSV infection cycle were significantly inhibited by nanomolar concentrations of the drug. It has been previously shown that inhibiting NMTs interferes with the infection of multiple human viruses, all of which are known to have myristoylated viral proteins [13-15]. The sequence of SARS-CoV-2 genome does not harbour obvious myristoylation sites. Although we did not investigate whether SARS-CoV-2 viral proteins are myristoylated, our results indicate that the infectivity of virions released from IMP-1088-treated cells is significantly compromised. This antiviral effect was retained even if the drug had been washed out from the cells before infection. Taken together, these results indicate that IMP-1088 is a good candidate for COVID-19 prophylaxis and treatment. The loss of

infectivity of the virions released from drug treated cells suggest that this antiviral strategy could potentially be beneficial in reducing the person-to-person transmissibility of infection, which would have an important impact in stalling the pandemic.

Materials and methods

Cells, drug treatments, and viruses

Human small lung carcinoma A549-AT cells transgenically expressing ACE2 and TMPRSS2-GFP (DOI 10.1101/2022.09.14.508057), and VeroE6[20] cells were maintained in Dulbecco's Modified Eagle's High Glucose Medium (DMEM, Merck, Cat. no. D6546), 1% L-glutamine (Gibco, Cat. no. 35050061), 1% non-essential amino acids (NEAA, Gibco, Cat. no. 11140050), 10% foetal bovine serum (FBS, Thermo Fisher Scientific, Cat. no. 10270-106), 1x penicillin and streptomycin (P/S, Merck, Cat. no. P0781) and incubated at 37 °C in 5% CO_2 atmosphere. All experiments analysed by imaging were performed in 96-well imaging plates (PerkinElmer, Cat. no. 6055302). Cells were seeded 24 h prior to infection at a density of 15.000 cells/well. The cells were treated with indicated concentrations of IMP-1088 (MedChemExpress, Cat. no. HY-112258), UCN-01 (Merck, Cat. no. 539644), or 4OH-Dynasore (Merck, Cat. no. D7693), at the indicated times before or after infection. The drug stocks (10 mM IMP-1088, 10 mM UCN-01, 100 mM 4OH-Dynasore) were prepared in DMSO (Merck, Cat. no. D2650), which was used in the experiments as vehicle control at a dilution correspondent to the amount of solvent contained in the highest concentration of each used drug. At indicated times after infection, cells were fixed and processed for indirect immunofluorescence detection of viral and cellular components (see Immunofluorescence staining below).

SARS-CoV-2 Wuhan (strain B.1), Delta (strain B.1.617.2) and Omicron (B.1.1.529) viruses were produced in Caco2 cells (passage 2) [20] in the biosafety level 3 (BSL-3) facility of the University of Helsinki under permits 30 HUS/32/2018§16. Cells were infected in DMEM supplemented with 2% FBS, 2 mM glutamine, 1xP/S, 20 mM HEPES, pH 7.2, at MOI=0.01. Media containing viruses collected at 48 hpi. After two centrifugations at 300xg and 3000xg, for 5 and 10 min, respectively, the cleared media were aliquoted and stored at – 80°C in the BSL3 premises. Viruses were tittered by standard plaque assay on VeroE6-TMPRSS2 [20]. Deep sequencing confirmed that all viruses had an intact furin cleavage site on the spike.

Immunofluorescence staining

The cells in 96-well plates were fixed with 4% paraformaldehyde (PFA, Merck, Cat. no. P6148) in phosphate buffered saline (PBS), at room temperature for 20 min. PFA was then replaced with PBS and all the plates were inactivated according to the institutional regulations using ultraviolet radiation (5000 J/m^2 dose, UVP Crosslinker model CL-1000, Analytikjena) before transferring the samples out of the BSL-3 facility. The excess fixative was blocked by

incubation with 50 mM ammonium chloride (NH_4Cl; Merck Cat. no. 254134) prepared in PBS at room temperature for 20 min. Cells were then permeabilized with 0.1% (weight/volume) Triton X-100 (Merck, Cat. no. X100) in PBS and the nuclei were stained with the DNA dye Hoechst 33342 (1 mg/ml, Thermo Fisher Scientific, Cat. no. 62249) in Dulbecco-modified PBS (Merck, Cat. no. D8662) supplemented with 0.2% BSA (Merck, Cat. no. 9048-46-8), here referred to as Dulbecco-BSA, for 10 min. The cells were then washed twice with Dulbecco-BSA and incubated with the primary antibodies diluted in Dulbecco-BSA at +4°C, overnight. On the following day, the cells were washed twice with Dulbecco-BSA and incubated with the secondary antibodies diluted in Dulbecco-BSA for 1 hour at room temperature covered from light. After two washes in Dulbecco-BSA, cells were imaged in PBS. Viral nucleocapsid (N) protein was detected with an in-house-developed rabbit polyclonal antibody raised against the viral N protein of SARS-CoV-2 (a kind gift from Dr. Jussi Hepojoki [20], University of Helsinki, Finland, dilution 1:2000). The mouse antibody against dsRNA (dilution 1:500) was from SCICONS (Cat. no. 10010500), Alexa Fluor 647-conjugated goat anti-rabbit and Alexa fluor 550-conjugated goat anti-mouse were from Thermo Fisher Scientific (Cat. no. A32733 and A32727, respectively). Actin was stained using Alexa Fluor-488 conjugated phalloidin (Invitrogen, Cat. no. A12379).

High-throughput imaging and automated image analysis

Automated fluorescence imaging was done using a Molecular Devices Image-Xpress Nano high-content epifluorescence microscope equipped with a 10× and 20x objective and a 4.7-megapixel CMOS (complementary metaloxide semiconductor) camera (pixel size, 0.332µm). Image analysis was performed with CellProfiler-4 software (http://www.cellprofiler.org). Automated detection of nuclei was performed using the Otsu algorithm inbuilt in the software. To automatically identify infected cells, an area surrounding each nucleus (5-pixel expansion of the nuclear area) was used to estimate the mean fluorescence intensity of the viral N or dsRNA immunolabeling in each cell, using an intensity threshold such that <0.01% of positive cells were detected in noninfected wells. On average, >30,000 cells per sample were analysed. The percentage of cells positive for the virus N-protein or dsRNA relative to the total number of detected nuclei was then quantified and plotted.

qRT-PCR

Viral RNA was extracted from 50 ml cell culture medium using QIAamp Viral RNA Mini Kit according to protocol provided by the manufacturer (Qiagen; Cat No. 52904). RNA concentration and quality were evaluated using NanoDrop 2000 Spectrophotometer (Thermo Fischer Scientific). The qRT-PCR was run in quadruplicate using TaqMan Fast Virus 1-step MasterMix (Thermo Fischer Scientific, Cat. no. 4444432). Primers and probes used for the

qRT-PRC reactions were ordered from Metabion international AG (www.metabion.com) as follows: RdRP-SARSr-F2: 5'- GTG ARA TGG TCA TGT GTG GCG G -3' forward primer, RdRP-SARSr-R2: 5' - CAR ATG TTA AAS ACA CTA TTA GCA TA – 3' reverse primer, RdRP-SARSr-P2: 5'- 6 - Fam - CAG GTG GAA CCT CAT CAG GAG ATG C -BHQ - 1 - 3' the probe. The qRT-PCR reaction was run with Agilent Technologies Stratagene Mx3005P using the following parameters: Reverse transcription for 5 min at 50°C, initial denaturation for 20 s at 95°C and amplification steps at 95°C for 3 s and 60°C for 30 s (the amplifications steps were repeated for 40 cycles).

Statistical analysis

Statistical analysis of the data was performed in GraphPad Prism 6. Two-tailed unpaired Student's t-test was performed when two conditions were compared. One-way ANOVA was used when more than two groups were analysed. When the main effect was found statistically significant, post-hoc Turkey's multiple comparisons tests were carried out. Differences were considered statistically significant when $p<0.05$. Data in figures are presented as mean ± SEM of at least three independent experiments.

Acknowledgments

This research was supported by the Academy of Finland (grant numbers 335527 to G.B., 351040 and 336490 to O.V., 339510 to T.Si., 321809 to T.St.), VEO—European Union's Horizon 2020 (grant number 874735 to O.V. and T.S.), the Jane and Aatos Erkko Foundation (to O.V. and T.Si.), the University of Helsinki Graduate Program in Microbiology and Biotechnology (R.O.), and European Union's Horizon Europe research and innovation program (grant umber 101057553 to G.B. and O.V.), Helsinki Institute for Life Sciences (HiLIFE, G.B. and O.V.), MJ is supported by The University of Queensland Amplify Fellowship, S.H.S. and N.Y. by the Australian Government Research Training Program (RTP) and Commonwealth Tuition Fee Offset Scholarship, and N.Y. by The Westpac Scholars Trust. The funders had no role in the study design, data collection and interpretation. High-throughput imaging was performed at Light Microscopy Unit of the University of Helsinki. The authors declare no competing interests.

Author contributions

M.J. and G.B. conceived the project. S.H.S., M.J. and G.B. planned the work. S.H.S. performed and analysed all experiments with support from R.O., T.Q., and T.St. O.V. and T.Si. provided reagents and coordinated the work in BSL3, and R.K. and L.K. assisted with the work in BSL3. S.H.S, M.J. and G.B. wrote the manuscript. N.Y. assisted in making the figures. All authors participated in proof-reading the manuscript and approved it for publication.

References

1 Hoffmann, M. *et al.* SARS-CoV-2 Cell Entry Depends on ACE2 and TMPRSS2 and Is Blocked by a Clinically Proven Protease Inhibitor. *Cell* **181**, 271-280 e278, doi:10.1016/j.cell.2020.02.052 (2020).

2 Jackson, C. B., Farzan, M., Chen, B. & Choe, H. Mechanisms of SARS-CoV-2 entry into cells. *Nat Rev Mol Cell Biol* **23**, 3-20, doi:10.1038/s41580-021-00418-x (2022).

3 Koch, J. *et al.* TMPRSS2 expression dictates the entry route used by SARS-CoV-2 to infect host cells. *EMBO J* **40**, e107821, doi:10.15252/embj.2021107821 (2021).

4 Yadati, T., Houben, T., Bitorina, A. & Shiri-Sverdlov, R. The Ins and Outs of Cathepsins: Physiological Function and Role in Disease Management. *Cells* **9**, doi:10.3390/cells9071679 (2020).

5 V'Kovski, P., Kratzel, A., Steiner, S., Stalder, H. & Thiel, V. Coronavirus biology and replication: implications for SARS-CoV-2. *Nat Rev Microbiol* **19**, 155-170, doi:10.1038/s41579-020-00468-6 (2021).

6 Wolff, G. *et al.* A molecular pore spans the double membrane of the coronavirus replication organelle. *Science* **369**, 1395-1398, doi:10.1126/science.abd3629 (2020).

7 Klein, S. *et al.* SARS-CoV-2 structure and replication characterized by in situ cryo-electron tomography. *Nat Commun* **11**, 5885, doi:10.1038/s41467-020-19619-7 (2020).

8 Farazi, T. A., Waksman, G. & Gordon, J. I. The biology and enzymology of protein N-myristoylation. *J Biol Chem* **276**, 39501-39504, doi:10.1074/jbc.R100042200 (2001).

9 Dian, C. *et al.* High-resolution snapshots of human N-myristoyltransferase in action illuminate a mechanism promoting N-terminal Lys and Gly myristoylation. *Nat Commun* **11**, 1132, doi:10.1038/s41467-020-14847-3 (2020).

10 Towler, D. A. *et al.* Purification and characterization of yeast myristoyl CoA:protein N-myristoyltransferase. *Proc Natl Acad Sci U S A* **84**, 2708-2712, doi:10.1073/pnas.84.9.2708 (1987).

11 Meinnel, T., Dian, C. & Giglione, C. Myristoylation, an Ancient Protein Modification Mirroring Eukaryogenesis and Evolution. *Trends Biochem Sci* **45**, 619-632, doi:10.1016/j.tibs.2020.03.007 (2020).

12 Maurer-Stroh, S. & Eisenhaber, F. Myristoylation of viral and bacterial proteins. *Trends Microbiol* **12**, 178-185, doi:10.1016/j.tim.2004.02.006 (2004).

13 Mousnier, A. *et al.* Fragment-derived inhibitors of human N-myristoyltransferase block capsid assembly and replication of the common cold virus. *Nat Chem* **10**, 599-606, doi:10.1038/s41557-018-0039-2 (2018).

14 Priyamvada, L. *et al.* Inhibition of vaccinia virus L1 N-myristoylation by the host N-myristoyltransferase inhibitor IMP-1088 generates non-infectious virions defective in cell entry. *PLoS Pathog* **18**, e1010662, doi:10.1371/journal.ppat.1010662 (2022).

15 Immerheiser, M. *et al.* Towards a broad-spectrum antiviral, the myristoyltransferase inhibitor IMP-1088 suppresses viral replication – the Yellow fever NS5 is myristoylated. *bioRxiv*, 2021.2003.2009.434547, doi:10.1101/2021.03.09.434547 (2021).

16 Kreutzberger, A. J. B. *et al.* SARS-CoV-2 requires acidic pH to infect cells. *Proc Natl Acad Sci U S A* **119**, e2209514119, doi:10.1073/pnas.2209514119 (2022).

17 Spuul, P., Balistreri, G., Kaariainen, L. & Ahola, T. Phosphatidylinositol 3-kinase-, actin-, and microtubule-dependent transport of Semliki Forest Virus replication complexes from the plasma membrane to modified lysosomes. *J Virol* **84**, 7543-7557, doi:10.1128/JVI.00477-10 (2010).

18 Krzyzaniak, M. A., Zumstein, M. T., Gerez, J. A., Picotti, P. & Helenius, A. Host cell entry of respiratory syncytial virus involves macropinocytosis followed by proteolytic

activation of the F protein. *PLoS Pathog* **9**, e1003309, doi:10.1371/journal.ppat.1003309 (2013).

19 Johannsdottir, H. K., Mancini, R., Kartenbeck, J., Amato, L. & Helenius, A. Host cell factors and functions involved in vesicular stomatitis virus entry. *J Virol* **83**, 440-453, doi:10.1128/JVI.01864-08 (2009).

20 Cantuti-Castelvetri, L. *et al.* Neuropilin-1 facilitates SARS-CoV-2 cell entry and infectivity. *Science* **370**, 856-860, doi:10.1126/science.abd2985 (2020).

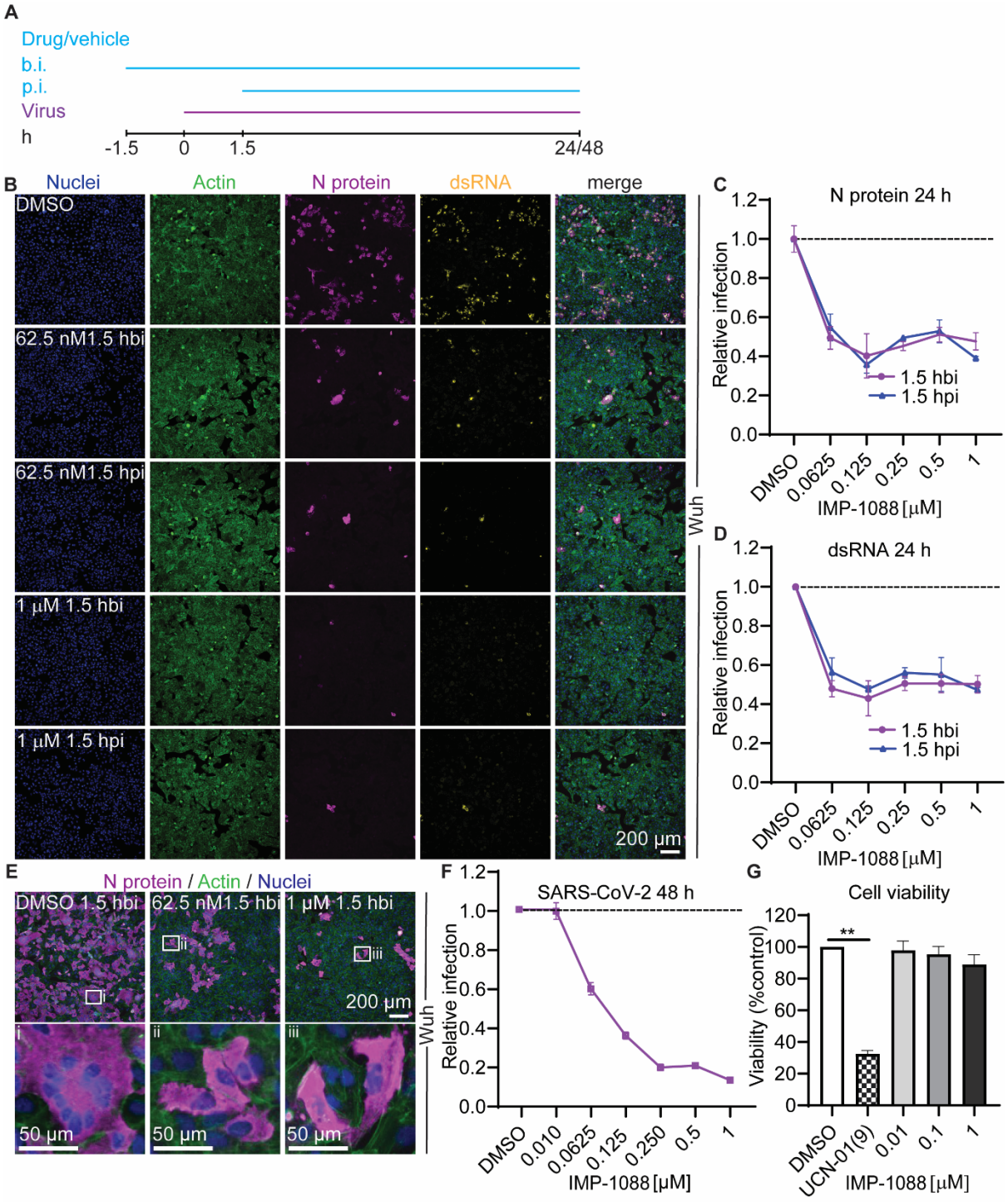

Figure 1. IMP-1088 inhibits SARS-CoV-2 infection at nanomolar concentrations. (**A**) Diagrammatic illustration of the experimental design. (**B**) Representative immunofluorescence images and (**C, D**) the quantification of the relative infection (the number of N-positive cells related to the number of nuclei in C, and number of dsRNA-positive cells/ number of nuclei in D) in A549-AT cells treated with indicated concentration of IMP-1088 or DMSO vehicle control, 1.5 hours before-infection (hbi) or post-infection (hpi), and infected with SARS-CoV-2 Wuh for 24 hours. Immunostainings show viral markers N (magenta) and dsRNA (yellow). Actin and nuclei are shown in green and blue, respectively. (**E**) Representative immunofluorescence images and (**F**) quantification of the relative infection in A549-AT cells treated with indicated concentration of IMP-1088 or DMSO vehicle control 1.5 hbi, and infected SARS-CoV-2 Wuh for 48 hours. Immunostainings show viral markers N (magenta). Actin and nuclei are shown in green and blue, respectively. The boxed areas i (multi-nucleated syncytium of cells), ii and iii (infected single cells) are shown magnified at the bottom of each image. (**G**) The quantification of cell viability of A549-AT cells treated with the indicated concentrations of the IMP-1088 or UCN-01 [9 μM], an inducer of apoptosis, for 24 h. All the results are normalised to DMSO vehicle controls and shown as mean ± SEM of 3 independent experiments. Statistical testing was performed with one-way ANOVA with Tukey's correction for multiple comparisons, **P<0.01.

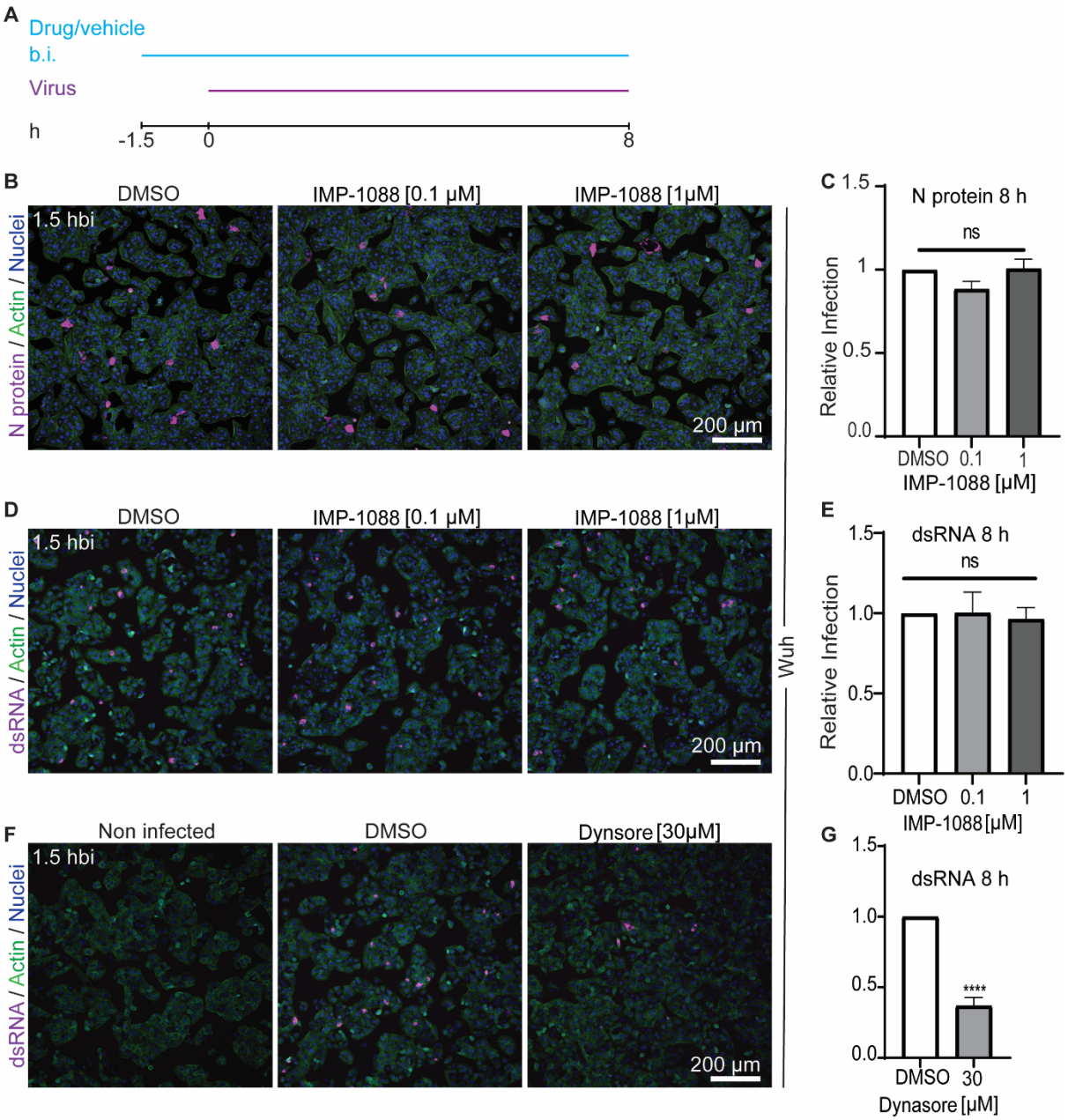

Figure 2. IMP-1088 does not inhibit SARS-CoV2 entry. (**A**) Diagrammatic illustration of the experimental design. (**B, D**) Representative immunofluorescence images and (**C, E**) the quantification of the relative infection (the number of N- positive cells related to the number of nuclei in (B,C), and number of dsRNA-positive cells/ number of nuclei in (D,E) in A549-AT cells treated with indicated concentration of IMP-1088 or DMSO vehicle control 1.5 hours before-infection (hbi) and infected SARS-CoV-2 Wuh for 8 hours. (**F**) Representative immunofluorescence images and (**G**) the quantification of the relative infection (the number of dsRNA-positive cells related to the number of nuclei in F) in A549-AT cells treated with 4OH-dynasore (30 μM) or DMSO vehicle control, 1.5 hours before-infection (hbi) and infected SARS-CoV-2 Wuh for 8 hours. Immunostaining shows viral marker N (magenta) and dsRNA (magenta). Actin and nuclei are shown in green and blue, respectively. The results are normalised to DMSO vehicle control and shown as mean ± SEM of 3 independent experiments. Statistical testing was performed with ordinary one-way ANOVA with Tukey's correction for multiple comparisons, ****$p<0.0001$; ns= non significant.

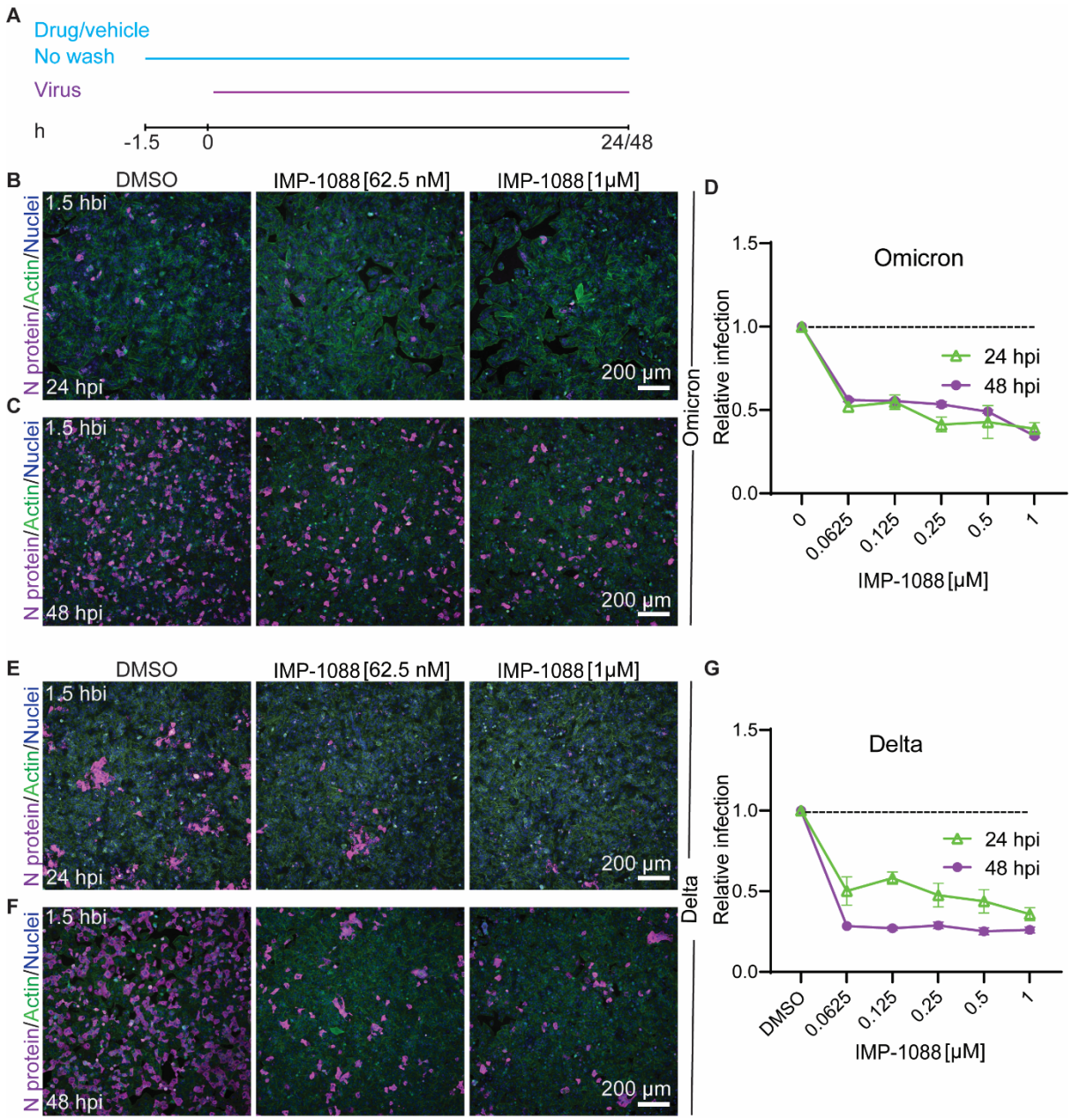

Figure 3. IMP-1088 inhibits infection of SARS-CoV-2 variants Omicron and Delta at nanomolar concentrations. (**A**) Diagrammatic illustration of the experimental design. (**B and C**) Representative immunofluorescence images of A549-AT cells infected with SARS-CoV-2 Omicron for 24 h (B) or 48 h (C) and treated with the indicated doses of IMP-1088 1.5 hours before-infection (hbi). (**D**) The quantification of the relative infection of SARS-CoV-2 Omicron at 24 h and 48 h post infection in A549-AT cells treated with the indicated doses of IMP-1088 or vehicle control (DMSO) at 1.5 hbi. (**E and F**) Representative immunofluorescence images of A549-AT cells infected with SARS-CoV-2 Delta for 24 h (E) or 48 h (F) and treated with the indicated doses of IMP-1088 1.5 hours hbi. (**G**) The quantification of the relative infection of SARS-CoV-2 Delta at 24 h and 48 h post infection in A549-AT cells treated with the indicated doses of IMP-1088 or vehicle control (DMSO) at 1.5 hbi. All the results are normalized to DMSO vehicle controls and shown as mean ± SEM of 3 independent experiments.

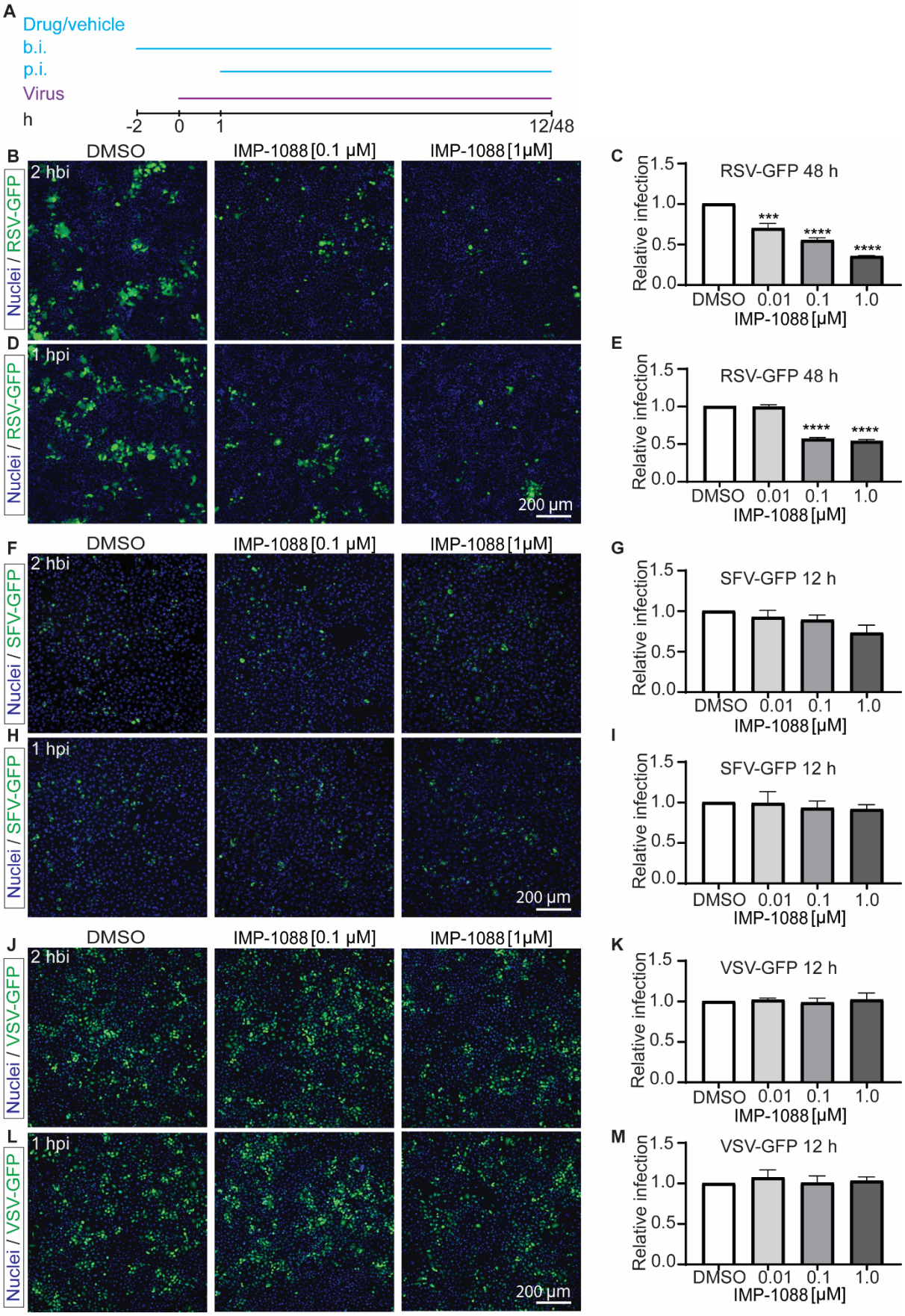

Figure 4. IMP-1088 inhibits Respiratory syncytial virus but not Semliki Forest nor Vesicular stomatitis virus infections. (**A**) Diagrammatic illustration of the experimental design. (**B**) Representative immunofluorescence images and (**C**) the quantification of the relative RSV-GFP (green) infection (the number of GFP positive cells related to the number of nuclei) at 48 hours post infection (hpi) in A549 cells treated with the indicated doses of IMP-1088 or vehicle control (DMSO) 2 hours before infection (hbi), or (**D and E**) 1 hpi. (**F**)

Representative immunofluorescence images and (**G**) the quantification of the relative SFV-GFP (green) infection (the number of GFP positive cells related to the number of nuclei) at 12 hpi in A549 cells treated with the indicated doses of IMP-1088 or vehicle control (DMSO) 2 hbi, or (**H and I**) 1 hpi. (**J**) Representative immunofluorescence images and (**K**) the quantification of the relative VSV-GFP (green) infection (the number of GFP positive cells related to the number of nuclei) at 12 hpi in A549 cells treated with the indicated doses of IMP-1088 or vehicle control (DMSO) 2 hbi, or (**L and M**) 1 hpi. All the results are normalised to DMSO vehicle controls and shown as mean ± SEM of 3 independent experiments. Nuclei are indicated in blue. Statical analysis was performed with one-way ANOVA with Tukey's correction for multiple comparisons, ***P<0.001, and ****P<0.0001.

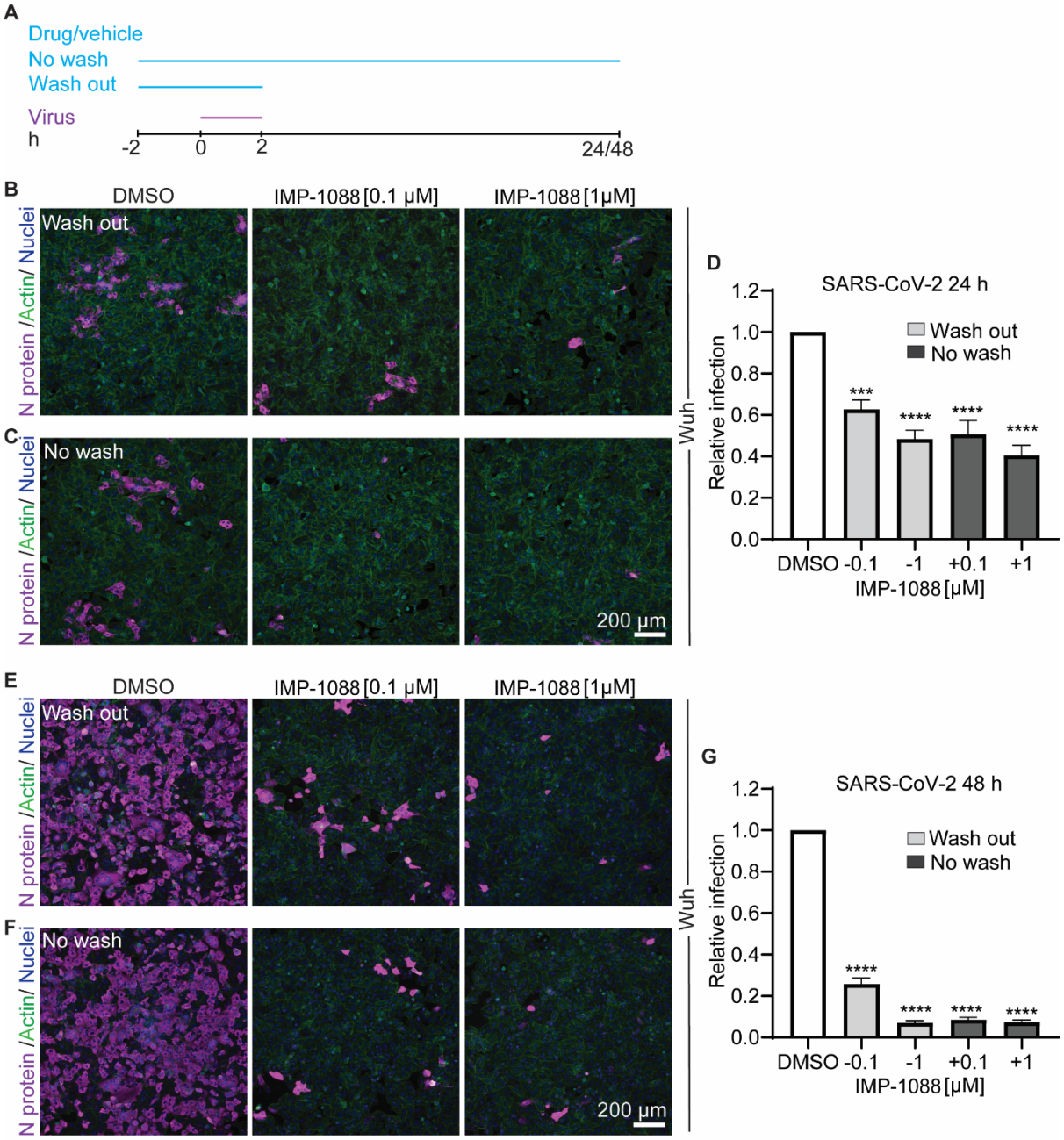

Figure 5. The reversibility of IMP-1088 antiviral activity is slow. (**A**) Diagrammatic illustration of the experimental design. (**B and C**) Representative immunofluorescence images and (**D**) the quantification of the relative SARS-CoV-2 Wuh (green) infection (the number of N-positive cells related to the number of nuclei) at 24 hpi in A549-AT cells treated with the indicated doses of IMP-1088 or vehicle control (DMSO) 2 hours before infection (hbi). The drug was then washed off (B, and "Wash out" in D) or left on the cell culture dish (C, and "No wash" in D) and the cells were infected with SARS-CoV-2 Wuh for 24 h, fixed and immunostained for N protein (magenta). Actin and nuclei are shown in green and blue, respectively. (**E and F**) Representative immunofluorescence images and (**G**) the quantification of the relative SARS-CoV-2 Wuh (green) infection (the number of N-positive cells related to the number of nuclei) at 48 hpi in A549-AT cells treated with the indicated doses of IMP-1088 or vehicle control (DMSO) 2 hours before infection (hbi). The drug was then washed off (E, and "Wash out"in G) or left on the cell culture dish (F, and "No wash" in G) and the cells were infected with SARS-CoV-2 Wuh for 48 h, fixed and immunostained for N protein (magenta). Actin and nuclei are shown in green and blue, respectively. All the results are normalised to DMSO vehicle controls and shown as mean ± SEM of 3 independent experiments. Statistical analysis was performed with one-way ANOVA with Tukey's correction for multiple comparisons, ***p<0.001, ****P<0.0001.

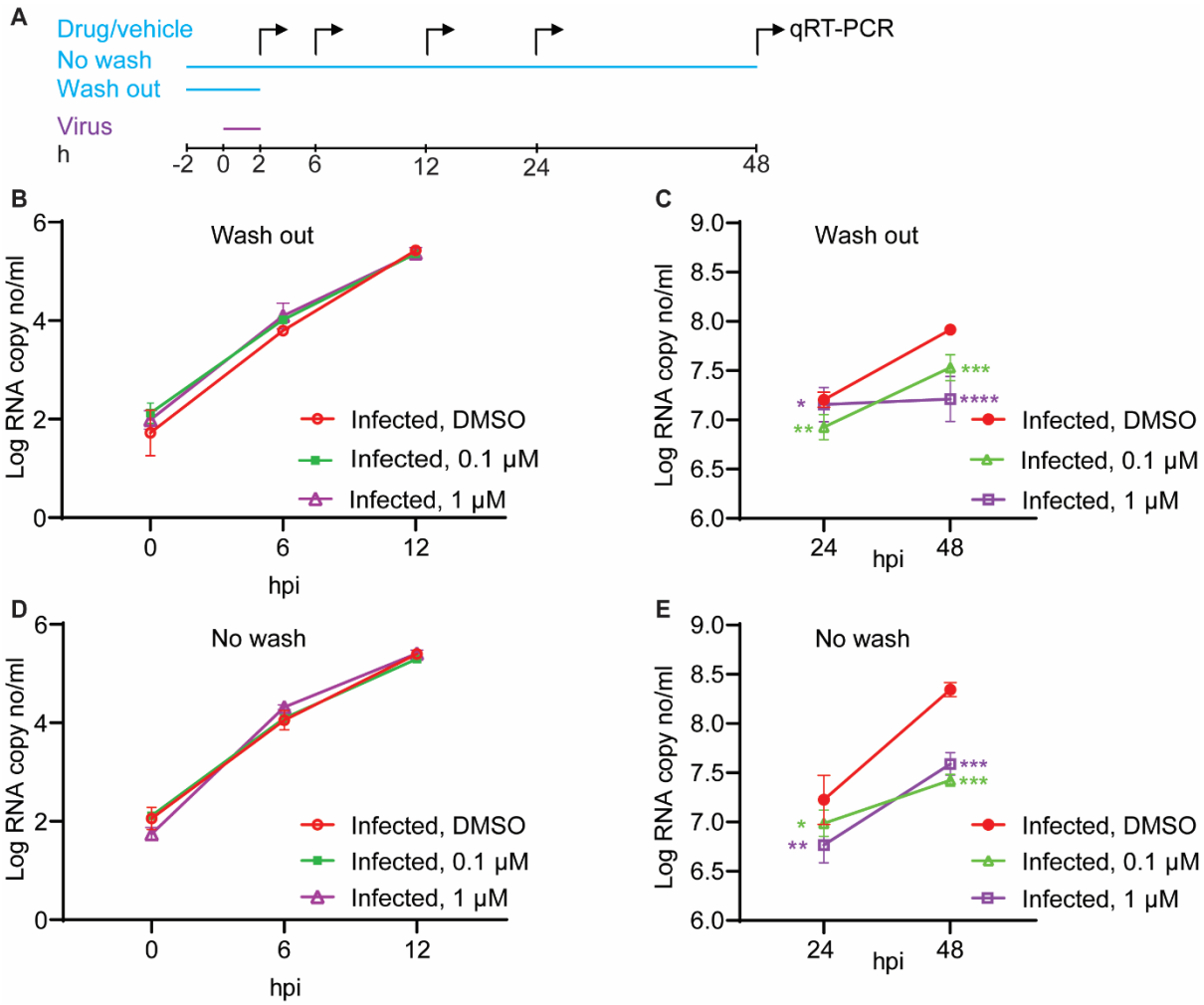

Figure 6. IMP-1088 does not impair the release of SARS-CoV-2 virions. (**A**) Diagrammatic illustration of the experimental design. A549-AT cells were treated with indicated concentrations of IMP-1088 or DMSO vehicle control at 2 hours before infection (hbi), and the drug was then either washed out (**B and C**) or left in the culture dish (**D and E**) and the cells were then infected with SARS-CoV-2 Wuh. The culture medium was collected at indicated time points (0 h to 48 h) for qRT-PCR detection of viral RNA. Note that C and E are shown from the same experiments shown in B and D, respectively. Statistical analysis was done using ordinary one-way ANOVA with Tukey's correction for multiple comparisons, *P<0.05, **P<0.01, ***P<0.001, ****P<0.0001. N = 4 technical replicates per concentration/time point.

A

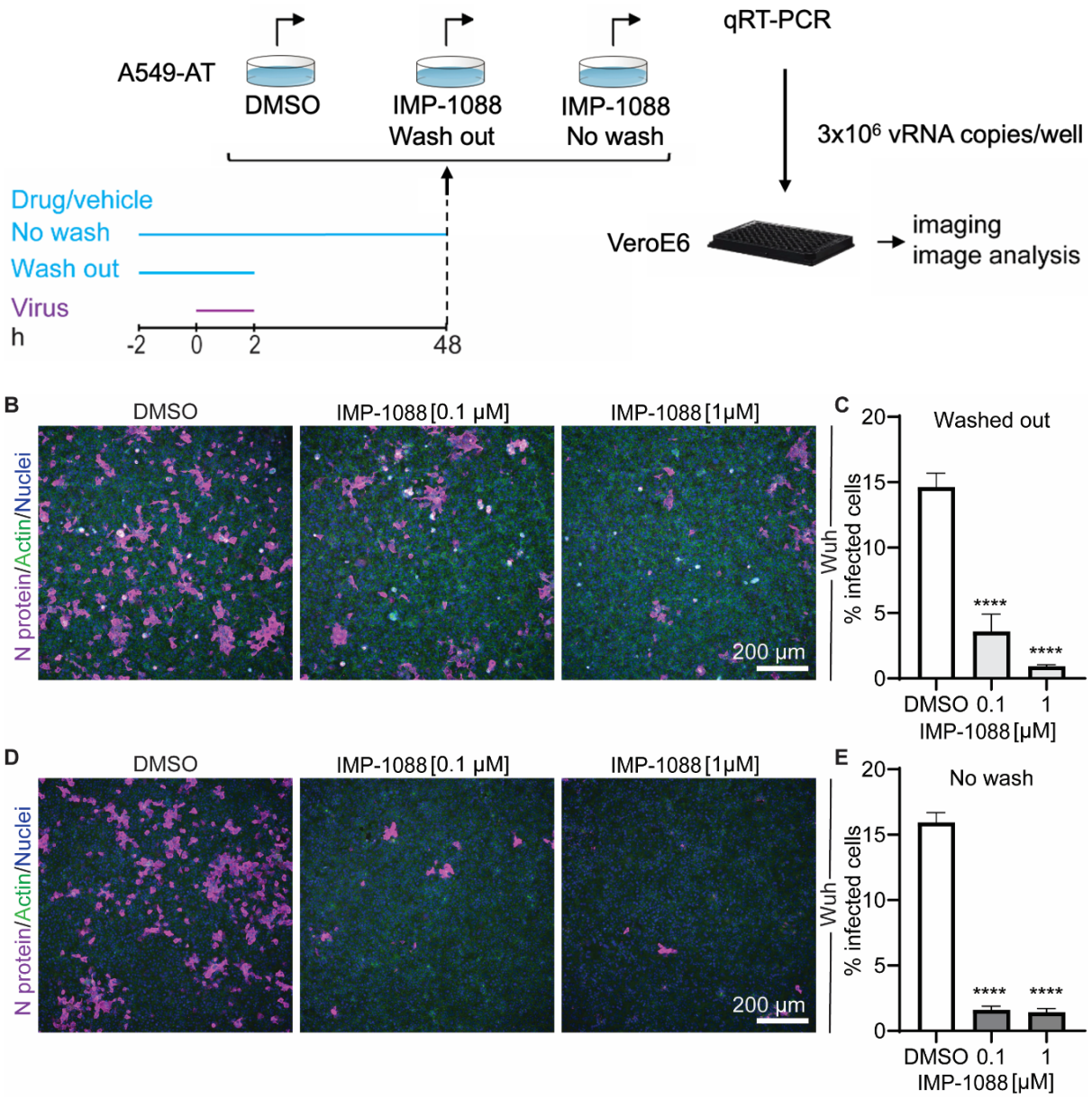

Figure 7. SARS-CoV-2 virions released from IMP-1088-treated cells are less infectious. (**A**) Diagrammatic illustration of the experimental design. (**B, D**) Representative immunofluorescence images and (**C, E**) the quantification of the relative SARS-CoV-2 Wuh (green) infection (the number of N-positive cells related to the number of nuclei) at 24 hours post infection (hpi) in VeroE6 cells. The viruses where isolated from A549-AT cells pre-treated with indicated IMP-1088 concentrations or DMSO, starting 2 hours before infection (hbi). Drugs were either washed out (B and C) or kept on cells for the duration of the experiment (D and E). VeroE6 cells were infected with inocula containing the same number of viral RNA genomes as measured by qRT-PCR. After infection for 20 h, VeroE6 cells were fixed and immunostained for N protein (magenta). Actin and nuclei are shown in green and blue, respectively. All the results are normalised to DMSO vehicle controls and shown as mean ± SEM of 3 independent experiments. Statistical analysis was performed with ordinary one-way ANOVA with Tukey's correction for multiple comparisons, ****P<0.0001.